



A facile method to prepare FeS/porous carbon composite as advanced anode material for lithium-ion batteries

Sheng-Ping Guo^{1,2,*}, Jia-Chuang Li¹, Ze Ma¹, Yang Chi¹, and Huai-Guo Xue^{1,*}

¹College of Chemistry and Chemical Engineering, Yangzhou University, Yangzhou 225002, Jiangsu, People's Republic of China

²State Key Laboratory of Structural Chemistry, Fujian Institute of Research on the Structure of Matter, Chinese Academy of Sciences, Fuzhou 350002, Fujian, People's Republic of China

Received: 29 August 2016

Accepted: 21 October 2016

Published online:
27 October 2016

© Springer Science+Business
Media New York 2016

ABSTRACT

Ferrous sulfide (FeS) particles dispersed in the pores of carbon (FeS/PC) from the polyacrylonitrile carbonization were prepared via a facile one-pot solid-state method, which was extensively characterized by XRD, SEM, TEM, Raman spectrum, and XPS techniques. As an anode material for lithium-ion batteries, this FeS/PC composite can achieve a high initial discharge capacity of 1428.8 mAh/g at 0.1 C, and can maintain 624.9 mAh/g capacity after 150 cycles. The porous carbon accommodates the volume change during the cycling, and the special structure of the FeS/PC composite results in its advanced electrochemical performance by enhancing the structure stability.

Introduction

As an important energy storage device, lithium-ion batteries (LIBs) have been widely used in electronic products because they have high energy density, are light-weight, and do not cause pollution [1–6]. However, the demand for improved electrochemical performance of LIBs is growing rapidly as the next generation of LIBs is expected to be used in power electric vehicles and smart grids to support the demand for low-carbon products [7, 8]. Researchers have exerted significant efforts to improve LIBs' performance and meet the requirements of social development [9–14]. As an important component of LIBs, anode materials are important in enhancing

LIBs' performance. To investigate anode materials, researchers mainly focus their attention on Si, Ge, Sn, SnO₂, Li₄Ti₅O₁₂, alloy, transition metal oxide, transition metal sulfide, and so on. Transition metal sulfides are abundant in nature, and their crystal structures can be stable in a wide temperature range; moreover, they have higher electronic conductivity than transition metal oxides [1, 15–20].

As a transition metal sulfide, ferrous sulfide has received particular research interest as an anode material for LIBs. Apart from the common advantages of transition metal sulfide, it has a much higher electrode potential (approximately 1.3 V compared with that of Li/Li⁺) than that of graphite (below 0.2 V vs. Li/Li⁺), which can effectively restrict the

Address correspondence to E-mail: spguo@yzu.edu.cn; chhgxue@yzu.edu.cn

SEI membrane formation that usually occurs below 1.0 V versus Li/Li⁺ [21, 22]. Yu et al. [23] reported that FeS nanodots in porous graphitic carbon nanowires could deliver the capacity of 609 mAh/g for the third cycles at 0.1 C. Xing et al. [24] found that FeS microsheet could exhibit a first discharge capacity of 772 mAh/g and maintained 677 mAh/g after the 20th cycle. Joo et al. [25] discovered that FeS on carbon nanofiber, as a LIB anode without current collector, had the first discharge capacity of 845.2 mAh/g at 50 mA/g. Luo et al. [26] reported that FeS nanoparticles wrapped in reduced graphene oxide could deliver the first capacity of 1357 and 978 mAh/g maintained after 40 cycles at 100 mA/g. These results show improved electrochemical performance of FeS. However, its performances should be continuously improved in view of its advantages and the practical requirements for LIBs, which are interesting and challenging.

In this study, we report a facile one-pot solid-state method to prepare FeS confined in the 3D matrix of porous carbon (carbonized polyacrylonitrile, or CPAN), namely FeS/PC composite. FeS/PC has an initial discharge capacity of 1428.8 mAh/g at 0.1 C, the highest value as far as we know, and 624.9 mAh/g capacity can be still remained after 150 cycles. The systematic characterizations and electrochemical study of FeS/PC composite anode material for LIBs are presented.

Experimental

Preparation of FeS/PC composite, pure FeS, and CPAN

All chemicals of analytical grade were directly used in the experiment and not purified further. The ferrous sulfide/porous carbon (FeS/PC) composite was prepared by heating Fe, S, and PAN with the weight ratios of 3:3:4 in an evacuated silica tube. The heating profile is designed as follows after many efforts. The quartz tube was heated from room temperature to 600 °C with the speed of 0.5 °C/min and homogenized at several intermediate temperatures for 2 h, respectively. After 12 h' reaction at 600 °C, the furnace was cooled down to 300 °C in 12 h. Accordingly, pure FeS and CPAN were prepared with the same method. More details about this preparation method can be found in our earlier work [27].

Material characterizations

Powder X-ray diffraction (PXRD, Bruker D8 Advance) technique to analyze the crystalline phases of the FeS/PC composite and pure FeS were collected at 40 kV and 100 mA for CuK α radiation ($\lambda = 1.5406 \text{ \AA}$) at a scan speed of 5°/min at room temperature. Energy-dispersive X-ray spectroscopy (EDS, Bruker, Quantax) was used to confirm the element content. The images of EDS element mapping show the distributions of Fe, S, C, and N for the FeS/PC composite. Field emission scanning electron microscopy (SEM, Hitachi S-4800II), high-resolution transmission electron microscopy (HRTEM, Tecnai G2 F30 S-TWIN), and transmission electron microscopy (TEM, Philips Tecnai12) were used to observe the surface morphology and size. Raman spectrum (Renishaw, Renishaw inVia) was used to analyze the chemical structures. X-ray photoelectron spectroscopy (XPS, Thermofisher Scientific, ESCALAB250Xi) was used to determine the chemical composition. Thermogravimetric analysis (Pyris 1 TGA) was used to determine the FeS content of FeS/PC at a heating rate of 10 °C/min in air from room temperature to 900 °C. Brunauer–Emmett–Teller (BET) surface area measurements were carried out by nitrogen adsorption and desorption using a Micromeritics ASAP 2020 HD88 analyzer at 77 K.

Electrochemical measurements

The electrodes of the FeS/PC composite and pure FeS were composed of 80 wt% active material, 10 wt% carbon black, and 10 wt% polyvinylidene fluoride (PVDF), respectively. Firstly, the slurry was prepared by stirring the mixture in a certain amount of *N*-methyl-2-pyrrolidone (NMP), and then coated the slurry onto a copper foil. After drying at 80 °C for 8 h and 120 °C for 12 h in a vacuum oven, the foil was cut into disks with diameter of 1.6 cm.

The cell assembly was carried out using a CR-2032-type coin cell with a Li foil as the counter and reference electrode, and a Celgard 2325 film as the separator. The electrolyte used was 1 M LiPF₆ in a mixed solvent of 1:1 DEC/EC. The cells were assembled in a glovebox (VAC-Omni 102283) filled with argon where oxygen and water contents were less than 1 ppm. Cyclic voltammetry (C–V) measurements were carried out on an electrochemical workstation (CHI660D) in 0.01–3 V at a scan rate of 0.5 mV/s.

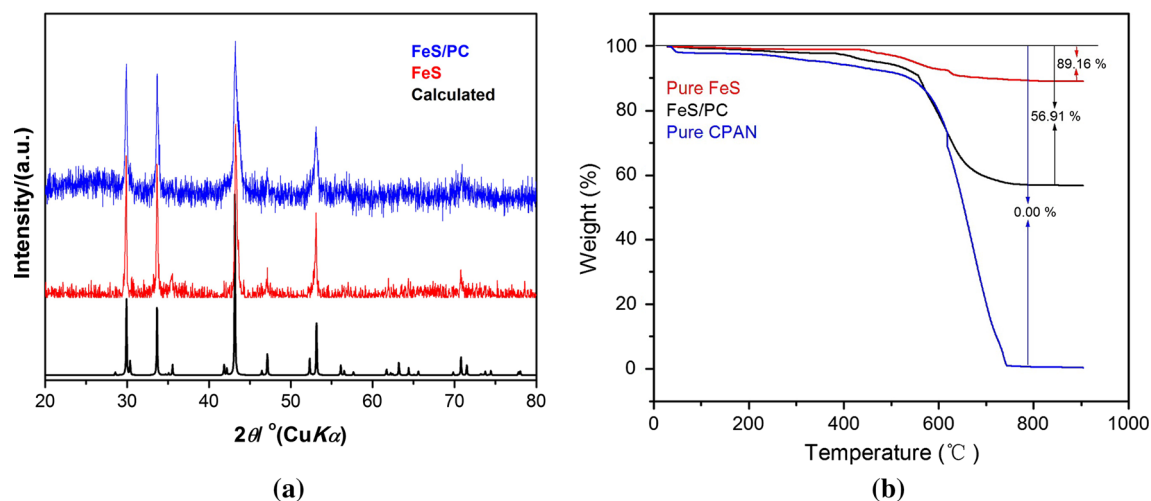


Figure 1 **a** Powdered XRD patterns of FeS/PC composite (blue) and pure FeS (red). The calculated one is obtained using the single-crystal structure data of FeS (ICSD No. 156618); **b** TGA curves of pure FeS, FeS/PC, and pure CPAN samples.

Electrochemical impedance spectroscopies (EIS) were measured over a frequency range of 0.01– 10^5 Hz. The galvanostatic charge/discharge tests were carried out at 0.1 C (60.9 mA/g) in the voltage range of 0.01–3 V using NEWARE CT-3008 battery charge–discharge system. The charge–discharge data were recorded after the first discharge to 0.01 V.

Results and discussion

Preparation of FeS/PC composite

Solid-state method is a normal choice to synthesize multinary metal chalcogenides, but it is unusual for synthesizing binary metal chalcogenides for energy-related applications. S and Fe elements are oxidized in the air when heated to high temperature; thus, FeS preparation has to be conducted under vacuum or inert gas protection. In addition, N-doped C-structure in CPAN is obtained when the reaction temperature is higher than 600 $^{\circ}\text{C}$ [27–31]. With the preceding considerations, we recently invented a facile preparation method to obtain MS/carbon (*M*: transition metal) composite to prepare FeS/PC composite, which has been successfully utilized to prepare SeS_x/CPAN composites [27]. Using this method, we finished FeS synthesis and PAN carbonization in one reactive system at the same time. Similar to the preparation of SeS_x/CPAN composites, heating profile has to be designed carefully when the reaction temperature is much higher than the sublimation

temperature of S. Then, some small gaseous molecules are produced from PAN carbonation. This one-pot method can be utilized to prepare other MS/carbon composites.

Structure and morphology characterizations

Figure 1a shows the PXRD patterns of FeS, the FeS/PC composite, and the calculated pattern of FeS. All diffraction peaks of FeS and FeS/PC are consistent with the calculated ones, indicating that obtained samples are pure FeS and FeS/PC, and FeS is crystallized with the hexagonal space group $P6-2c$ (No. 190). Besides, the FeS content in FeS/PC composite is calculated to be around 63% according to Fe_2O_3 mass formed by TGA analysis (Fig. 1b). EDS element analysis of the FeS/PC composite indicates that C, N, Fe, and S all exist, and that Fe and S ratio is around 1:1. The EDS element mapping analysis (Fig. 2) reveals that the C-element mapping image overlaps with those of S, Fe, and N, thereby demonstrating the uniform distribution of FeS in the N-doped C-matrix.

The Raman spectrum of the FeS/PC composite is shown in Fig. 3. The peaks at 1367.03 and 1586.65 cm^{-1} are D-band and G-band, respectively, indicating that partial C from PAN is graphitized after heat treatment. The large intensity ratio between the D and G bands ($I_D: I_G = 1.45$) shows that defects exist on the C surface, which is consistent with the appearance of pores on the CPAN surface [26].

The chemical composition and valence of FeS/PC composite were determined through XPS (Fig. 4).

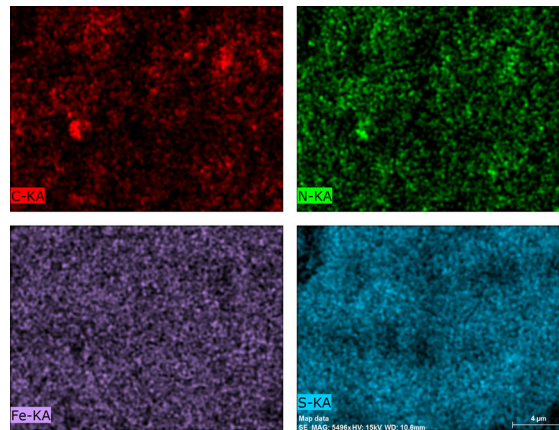
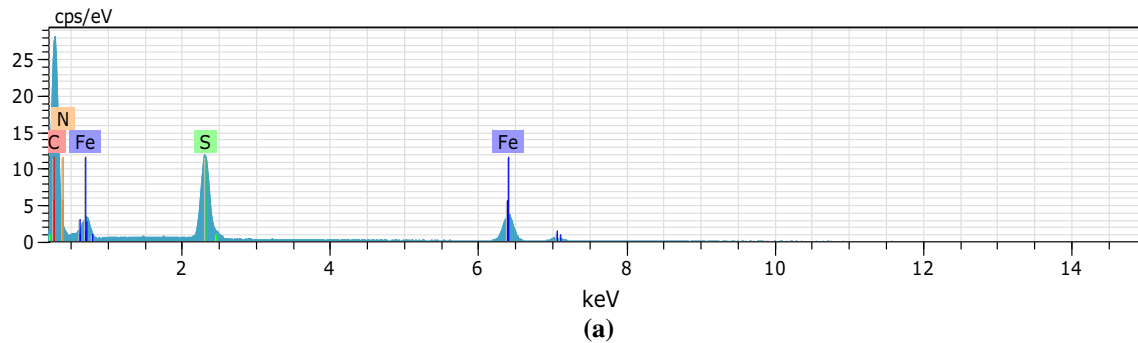


Figure 2 a EDS analysis for FeS/PC composite; b EDS elemental mapping images for C, N, Fe, and S in FeS/PC composite.

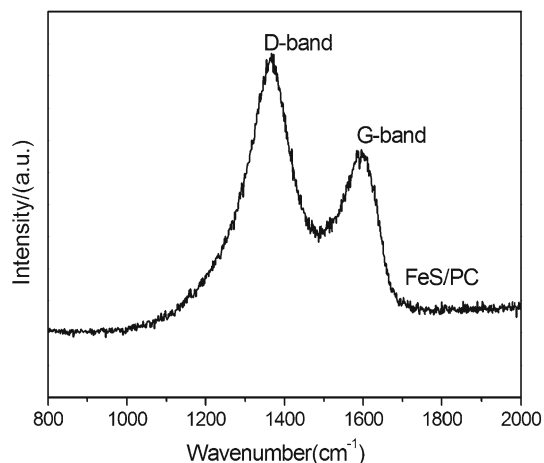


Figure 3 Raman spectrum of FeS/PC composite.

The N 1s spectrum (Fig. 4a) exhibits two characteristic peaks located at 398.58 and 400.48 eV, corresponding to the pyridinic and graphitic N, respectively [32]. The strong C 1s spectrum (Fig. 4b) further shows C=C, C=N, C–N, and C–C bonds, which are located at 287.68, 286.58, 284.78, and 284.48 eV, respectively. The Fe 2p (Fig. 4c) spectrum

has two peaks at 709.08 and 724.78 eV, which proves that Fe is divalent in the sample. The S 2p spectrum (Fig. 4d) also has two distinct peaks at 161.48 and 163.78 eV, which is consistent with those of the S^{2-} spectrum. All these XPS peaks prove that the sample is the composite of FeS and N-doped C, which agrees with the results of PXRD, EDS, SEM element mapping, and Raman spectrum.

The SEM images of the FeS/PC composite, pure CPAN, and pure FeS are shown in Fig. 5. Both pure FeS (Fig. 5a) and pure CPAN (Fig. 5b) particles are aggregated into blocks with uneven sizes. For FeS/PC composite, the CPAN surface has many pores with size ranging from scores of nm to around 200 nm, and FeS particles disperse in these pores or on the surface of the CPAN matrix (Fig. 5c). Therefore, as their SEM images suggest, adding PC to FeS can effectively reduce FeS particle aggregation. Also, as the TEM (Fig. 5d) and HERTEM (Fig. 5e) images show, some FeS particles disperse with sheet-like CPAN. In addition, the porous structure of FeS/PC was further investigated using N_2 adsorption/desorption analysis (Fig. 5f). The hysteresis loop for FeS/PC composite corresponds to the

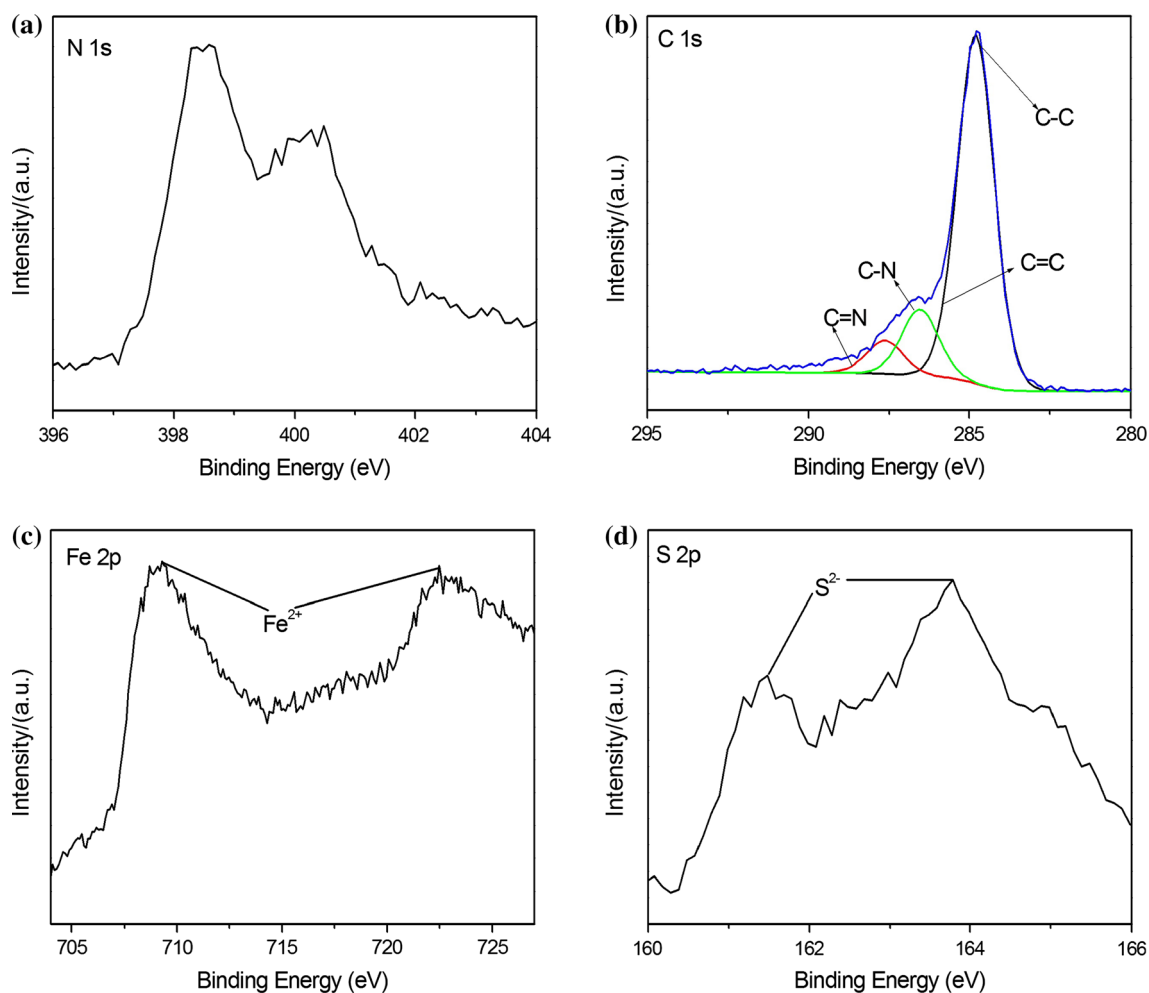


Figure 4 XPS spectra of FeS/PC composite: **a** N 1 s; **b** C 1 s; **c** Fe 2p; **d** S 2p.

Type-IV isotherm, which indicates that the sample has a mesoporous structure. The Brunauer–Emmett–Teller (BET)-specific surface area was measured to be about 226 m²/g, and the distribution of pore size was mainly centered at 10–20 nm.

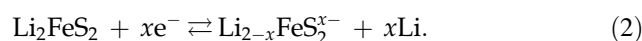
Electrochemical performance

Cyclic voltammetry (C–V) measurement is completed to analyze the redox reaction mechanism. The first three cycles for pure FeS and FeS/PC composite are recorded in Figs. 6a, b. For pure FeS (Fig. 6a), the reduction peak is found at 0.97 V for the first cycle, which could be explained by the following reaction [21, 33]:



The broad peak at 2.25 V is due to the oxidation reaction from Fe to Li_{2–x}FeS₂ [33]. After the first cycle,

the peaks that appeared indicate that the redox reaction is different. One peak at 0.45 V is relevant to the reduction reaction from Li_{2–x}FeS₂ to Li₂FeS₂ [26, 33]. The reduction peak at 0.97 V, however, disappeared after the first cycle. The oxidation peak moved to 2.2 V after the first cycle, which indicated the beginning of the delithiation process (Li₂FeS₂ to Li_{2–x}FeS₂) [26, 33, 34].



The first cycle's C–V curve of the FeS/PC composite is similar to that of pure FeS (Fig. 6b). However, the former shows considerably small changes in the following cycles. The near overlapping of all curves suggests the excellent reversibility of the electrochemical reactions and advanced structure stability [35]. The C–V curves of FeS/PC composite after 100 cycles are reported in Fig. 6c. The reduction peak at 0.97 V for the first three cycles moves to

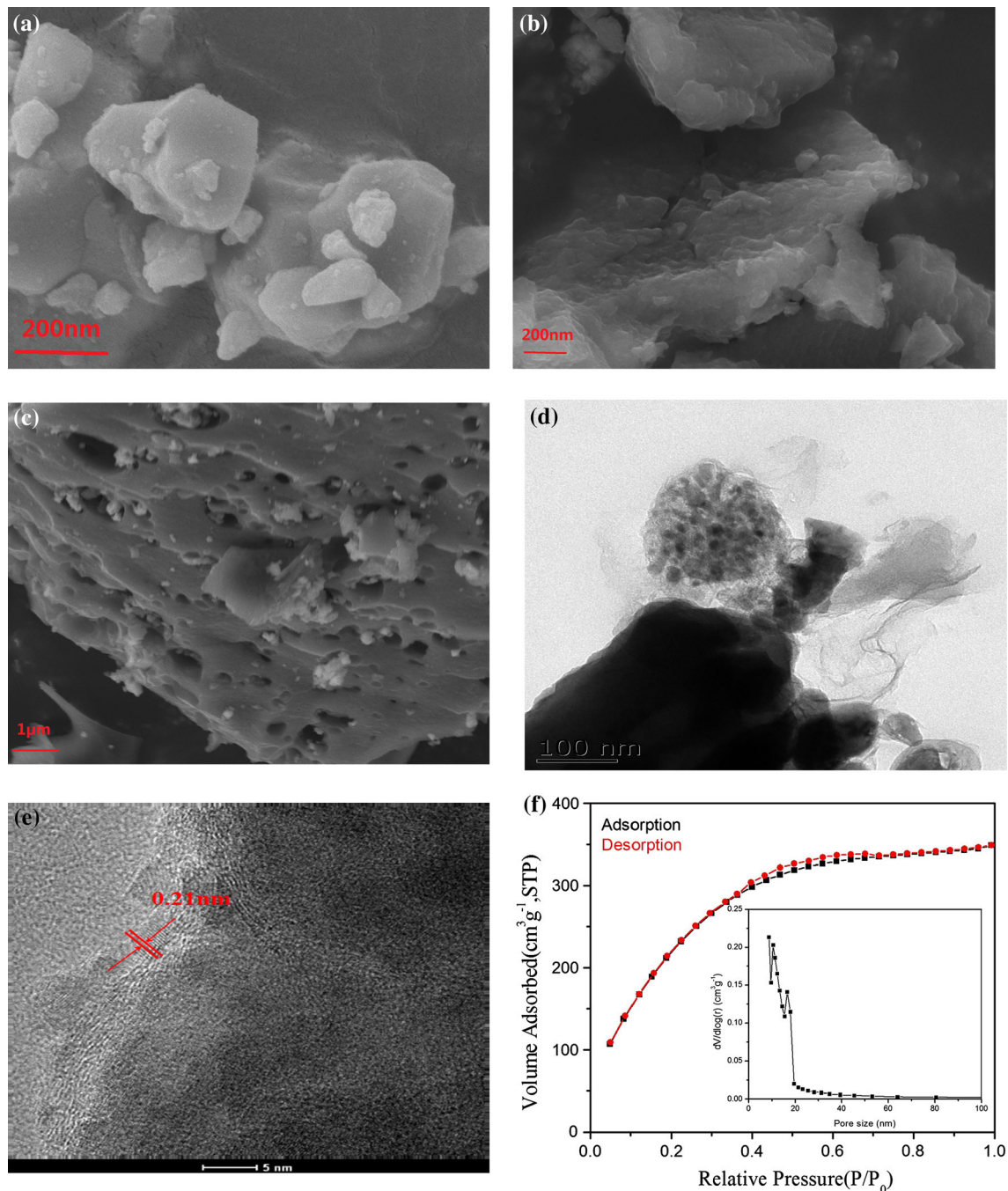


Figure 5 SEM images of pure FeS (a), pure CPAN (b), and FeS/PC composite (c); TEM image of FeS/PC composite (d); HRTEM image of FeS/PC composite (e); Nitrogen adsorption–desorption isotherm and pore size distribution of FeS/PC composite (f).

1.35 V after 100 cycles, which can also be attributed to Li_2FeS_2 formation, while the peak at 2.2 V is replaced by that at 2.0 V [36]. Compared with other C–V results [21, 23–26, 33], ours are a little different because of the unique preparation method, and the exact explanation may need support from some in-situ techniques.

Electrochemical impedance spectroscopies of pure FeS and FeS/PC composite (Fig. 7) are measured to analyze their interface performance. The semicircle radius of FeS/PC composite is significantly smaller than that of pure FeS as π -conjugated units of C=N, C=C, C–N, and C–C bonds which can effectively improve the electrical conductivity of

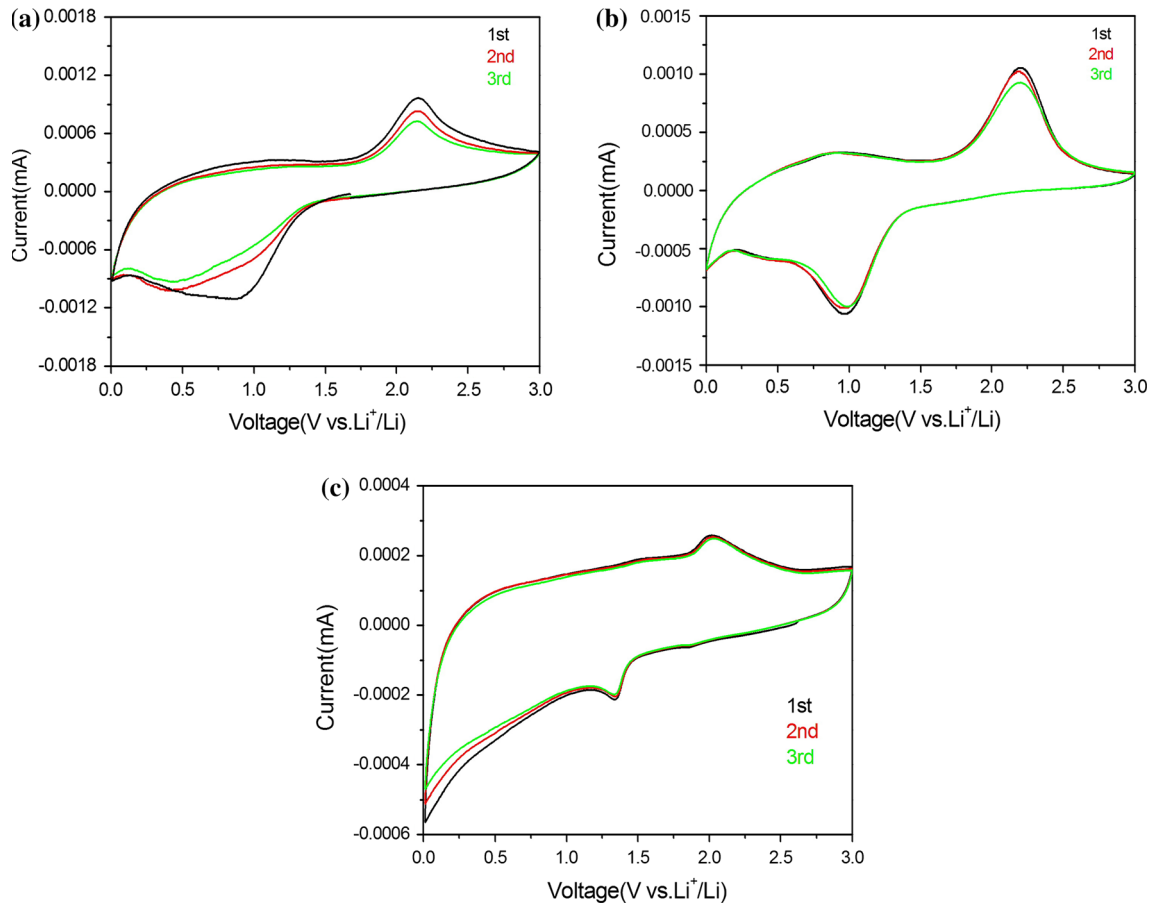


Figure 6 The C–V curves for fresh pure FeS (a), fresh FeS/PC (b), and FeS/PC after 100 cycles (c) for the first three cycles.

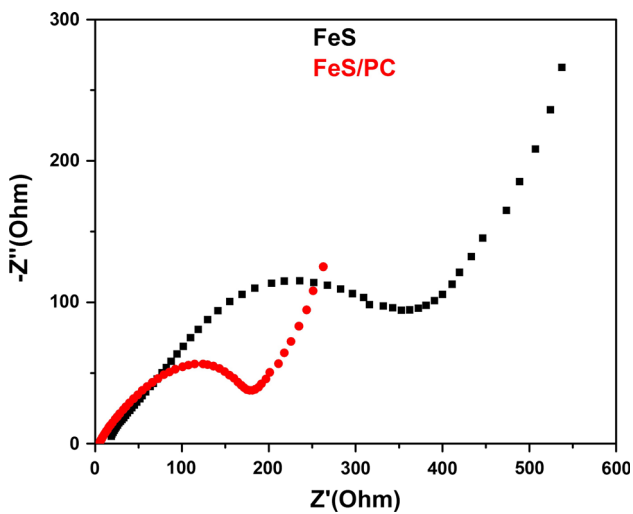


Figure 7 Nyquist plots for FeS/PC composite and pure FeS in frequency range of 0.01–10⁵ Hz.

the FeS/PC composite [37–39]. In addition, the straight line of the low-frequency region is approximately 45°, indicating better Li⁺ ion

diffusion for the FeS/PC composite electrode than that for pure FeS.

Stable cyclic performance of the electrode material is important for its practical application. The cycling stabilities of the FeS/PC composite (Fig. 8a) and pure FeS (Fig. 8b) electrodes are examined at 0.1 C between 0.01 and 3.0 V. The composite delivers a considerably high initial discharge capacity of 1428.8 mAh/g, which is so far the highest for FeS and significantly exceeds the theoretical capacity of FeS. The first charge capacity is only 1100.0 mAh/g. This indicates an irreversible capacity loss of 328.8 mAh/g, around 23.0% of the first discharge capacity, which can be explained by SEI layer formation [26]. In comparison, the initial discharge capacity of the pure FeS electrode prepared under the same conditions is only 796.3 mAh/g. The reason for this ultra-high capacity may be attributed to the capacity contribution of the N-doped PC matrix as the graphitized carbon can intercalate and de-intercalate Li⁺ ions. After the first cycle, the Coulombic efficiency is close

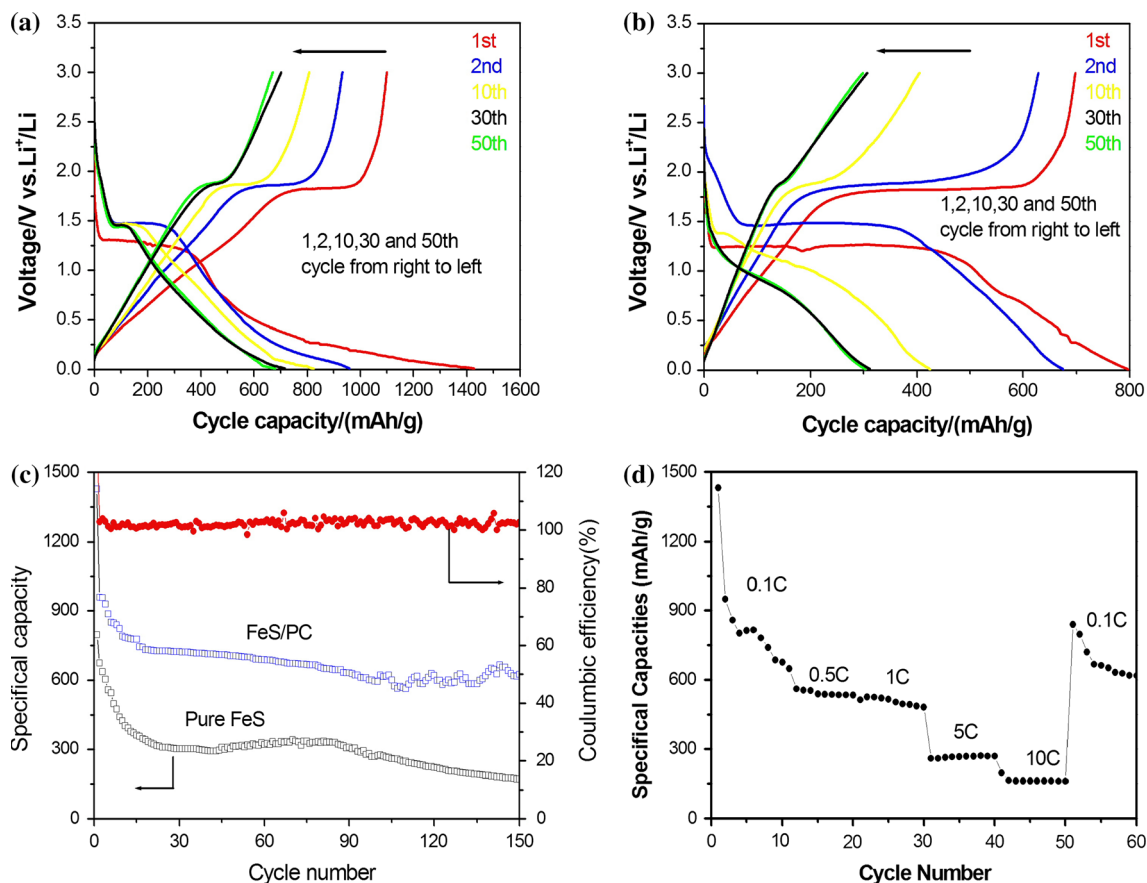


Figure 8 The charge and discharge curves of FeS/PC composite (a) and pure FeS (b) electrodes during the initial 50 cycles; c cyclic stability of FeS/PC composite and pure FeS electrodes for

150 cycles at 0.1 C; and d rate capabilities of FeS/PC composite at various current densities.

to 100% for all the 150 cycles, thereby demonstrating its reversibility. The FeS/PC composite still has a capacity of 678.8 mAh/g and a Coulombic efficiency approaching 99.9% after the 50th cycle, which is more than twice the capacity of 312.2 mAh/g for pure FeS. As shown in Fig. 8c, the FeS/PC composite exhibits a discharge capacity of 624.9 mAh/g after 150 cycles, which is approximately 67.2% of the second capacity. This promising cycling stability shows that the graphitization of carbon can help enhance the experimental capacity and protect the structure of FeS/PC composite from the damage during charge and discharge. The FeS/PC composite prepared by one-pot solid-state method has the enhanced capacity that exceeds those reported by previous studies [40–42]. Recent developments on the electrochemical data of FeS are summarized in Table 1. Almost all the other methods to synthesize FeS or its composite with

various carbon materials employ wet-chemical methods, while ours are solid-state one. Compared to the liquid method, the solid-state method is closer to large-scale industrial production, although shape control and size reduction are less available. Compared to the results shown in Table 1, the electrochemical data on FeS/PC are satisfactory; therefore, developing electrode materials for energy-related application using the pure solid-state method seems reasonable.

To elucidate the advantage of FeS/PC composite in lithium storage, its rate capabilities are determined (Fig. 8d). The specific capacities are decreased along with the increase of discharge/charge rates from 0.1 to 10 C. The fifth-cycle discharge capacities remain at 813.7, 537.6, 515.7, 266.4, and 162.0 mAh/g at 0.1, 0.5, 1, 5, and 10 C, respectively. These results reveal that incorporating CPAN into pure FeS can enhance its rate performance [25, 44].

Table 1 Recent reports on the electrochemical data of FeS as anode material for lithium-ion batteries

Material and morphology	Preparation method	Electrode formulation	Voltage window (V)	Current density (mA/g)	Initial discharge capacity (mAh/g)	Remained capacity after <i>n</i> cycles (mAh/g)	References
FeS@C nanosheet	Solvothermal method	80:10:10	0.01–3.0	100	1022	615/100	[33]
FeS@RGO nanoparticle	Ionic liquid assisted solid-state method	70:20:10	0.005–3	100	1357	978/40	[26]
FeS@TiO ₂ nanosheet	Hydrothermal method	70:20:10	0.01–3	100	1145	635/100	[21]
FeS@CNFs nanofiber	Electrostatic spinning	100:0:0	0.01–3	500	845.2	535.1/200	[25]
FeS microsheet	Hydrothermal method	100:0:0	0.01–3	100	772	677/20	[24]
FeS nanodots	Electrostatic spinning	70:20:10	1–3	61	579 (2 nd value)	400/50 at 305 mA/g	[23]
FeS@C microwire	Hydrothermal method	80:10:10	1.0–2.6	91	699	423/100	[41]
Porous FeS/C nanosheet	Freeze-drying/carbonization method	80:10:10	0.01–3.0	1000	1258	703/150	[43]
FeS/PC	One-pot solid-state method	80:10:10	0.01–3	61	1428.8	624.9/150	Our result

Conclusions

A novel FeS/PC composite was successfully prepared using a facile one-pot solid-state method. This composite has the highest initial discharge capacity of 1428.8, and 624.9 mAh/g capacity could still remain after 150 cycles. Furthermore, the composite showed perfect Coulombic efficiency and enhanced rate capability. The advanced electrochemical performance is attractive for LIB development with high power densities.

Acknowledgements

We gratefully acknowledge the financial support by National Natural Science Foundation of China (Grant No. 21673203), the Higher Education Science Foundation of Jiangsu Province (No. 15KJB150031), State Key Laboratory of Structural Chemistry Fund (No. 20150009), Natural Science Foundation of Yangzhou (No. YZ 2016122), the Priority Academic Program Development of Jiangsu Higher Education Institutions and the Qing Lan Project. We would also like to acknowledge the technical support received from the Testing Center of Yangzhou University.

References

- [1] Rui XH, Tan HT, Yan QY (2014) Nanostructured metal sulfides for energy storage. *Nanoscale* 17:9889–9924
- [2] Liu X, Zhang K, Lei KX, Li FJ, Tao ZL, Chen J (2016) Facile synthesis and electrochemical sodium storage of CoS₂ micro/nano-structures. *Nano Res* 9:198–206
- [3] Evans T, Piper DM, Kim SC, Han SS, Bhat V, Oh KH, Lee SH (2014) Ionic liquid enabled FeS₂ for high-energy-density lithium-ion batteries. *Adv Mater* 26:7386–7392
- [4] Douglas A, Carter R, Oakes L, Share K, Cohn AP, Pint CL (2015) Ultrafine iron pyrite (FeS₂) nanocrystals improve sodium-sulfur and lithium-sulfur conversion reactions for efficient batteries. *ACS Nano* 9:11156–11165
- [5] Liu J, Wen Y, Wang Y, Aken PAV, Maier J, Yu Y (2014) Carbon-encapsulated pyrite as stable and earth-abundant high energy cathode material for rechargeable lithium batteries. *Adv Mater* 26:6025–6030
- [6] Wu QH, Chen M, Chen KY, Wang SS, Wang CJ, Diao GW (2016) Fe₃O₄-based core/shell nanocomposites for high-performance electrochemical supercapacitors. *J Mater Sci* 51:1572–1580. doi:10.1007/s10853-015-9480-4
- [7] Zeng ZY, Zhang XW, Bustillo K, Niu KY, Gammer C, Xu J, Zheng HM (2015) In situ study of lithiation and delithiation of MoS₂ nanosheets using electrochemical liquid cell transmission electron microscopy. *Nano Lett* 15:5214–5220

- [8] Xiong FY, Cai ZY, Qu LB, Zhang PF, Yuan ZF, Asare OK, Xu WW, Lin C, Mai LQ (2015) Three-dimensional crumpled reduced graphene oxide/MoS₂ nanoflowers: a stable anode for lithium-ion batteries. *ACS Appl Mater* 7:12625–12630
- [9] Tarascon JM, Armand M (2001) Alternative energy technologies. *Nature* 414:359–367
- [10] Goodenough JB, Park KS (2013) The Li-ion rechargeable battery: a perspective. *J Am Chem Soc* 135:1167–1176
- [11] Vogt LO, Kazzi ME, Berg EJT, Villar SP, Novák P, Villeveille C (2015) Understanding the interaction of the carbonates and binder in Na-ion batteries: a combined bulk and surface study. *Chem Mater* 27:1210–1216
- [12] Kim SW, Seo DH, Ma XH, Ceder G, Kang K (2012) Electrode materials for rechargeable sodium-ion batteries: potential alternatives to current lithium-ion batteries. *Adv Energy Mater* 2:710–721
- [13] Palomares V, Cabanas MC, Martínez EC, Han MH, Rojo T (2013) Update on Na-based battery materials. A growing research path. *Energy Environ Sci* 6:2312–2337
- [14] Wang L, Lu YH, Liu J, Xu MW, Cheng JG, Zhang DW, Goodenough JB (2013) A superior low-cost cathode for a Na-ion battery. *Angew Chem Int Ed* 52:1964–1967
- [15] Slater MD, Kim DH, Lee E, Johnson CS (2013) Sodium-ion batteries. *Adv Funct Mater* 23:947–958
- [16] Fei F, Jiang YF, Xu Y, Chen G, Li YL, Xu X, Deng SG, Luo HM (2014) A novel solvent-free thermal reaction of ferrocene and sulfur for one-step synthesis of iron sulfide and carbon nanocomposites and their electrochemical performance. *J Power Sources* 265:1–5
- [17] Xie J, Liu SY, Cao GS, Zhu TJ, Zhao XB (2013) Self-assembly of CoS₂/graphene nanoarchitecture by a facile one-pot route and its improved electrochemical Li-storage properties. *Nano Energy* 2:49–56
- [18] Choi SH, Ko YN, Lee JK, Kang YC (2015) 3D MoS₂-graphene microspheres consisting of multiple nanospheres with superior sodium ion storage properties. *Adv Funct Mater* 25:1780–1788
- [19] Zhu CB, Wen YR, Aken PAV, Maier J, Yu Y (2015) High lithium storage performance of FeS nanodots in porous graphitic carbon nanowires. *Adv Funct Mater* 25:2335–2342
- [20] Chen M, Shen X, Wu QH, Li W, Diao GW (2015) Template-assisted synthesis of core-shell α -Fe₂O₃@TiO₂ nanorods and their photocatalytic property. *J Mater Sci* 50:4083–4094. doi:10.1007/s10853-015-8964-6
- [21] Wang XF, Xiang QY, Liu B, Wang LJ, Luo T, Chen D, Shen GZ (2013) TiO₂ modified FeS nanostructures with enhanced electrochemical performance for lithium-ion batteries. *Sci Rep* 3:2007
- [22] Liao F, S'wiatowska J, Maurice V, Seyeux A, Klein LH, Zanna S, Marcus P (2013) Electrochemical lithiation and passivation mechanisms of iron monosulfide thin film as negative electrode material for lithium-ion batteries studied by surface analytical techniques. *Appl Surf Sci* 283:888–899
- [23] Zhu CB, Wen YR, Yu Y (2015) High lithium storage performance of FeS nanodots in porous graphitic carbon nanowires. *Adv Funct Mater* 25:2335–2342
- [24] Xing CC, Zhang D, Cao K, Zhao SM, Wang X, Qin HY, Liu JB, Jiang YZ, Meng L (2015) In situ growth of FeS microsheet networks with enhanced electrochemical performance for lithium-ion batteries. *J Mater Chem A* 3:8742–8749
- [25] Fei L, Williams BP, Yoo SH, Carlin JM, Joo YL (2016) A general approach to fabricate free-standing metal sulfide@carbon nanofiber networks as lithium ion battery anodes. *Chem Commun* 52:1501–1504
- [26] Fei L, Lin QL, Yuan B, Chen G, Xie P, Li YL, Xu Y, Deng SD, Smirnov S, Luo HM (2013) Reduced graphene oxide wrapped FeS nanocomposite for lithium-ion battery anode with improved performance. *ACS Appl Mater* 5:5330–5335
- [27] Guo SP, Li CX, Chi Y, Ma Z, Xue HG (2016) Novel 3-D network SeS_x/NCPAN composites prepared by one-pot in situ solid-state method and its electrochemical performance as cathode material for lithium-ion battery. *J Alloys Compd* 664:92–98
- [28] Guo SP, Guo GC (2014) Crystal structure and magnetic and photocatalytic properties of a new ternary rare-earth mixed chalcogenide, Dy₄S₄Te₃. *J Mater Chem A* 2:20621–20628
- [29] Guo SP, Wang GE, Zhang MJ, Wu MF, Liu GN, Jiang XM, Guo GC, Huang JS (2013) Novel single-crystal's voltage-dependent effect and magnetic order of Ln₂ZrQ₅ (Ln = La, Sm, Gd; Q = S, Se) semiconductors. *Dalton Trans* 42:2679–2682
- [30] Guo SP, Chi Y, Xue HG (2015) Sm₃S₃BO₃: the first sulfide borate without S–O and B–S bonds. *Inorg Chem* 54:11052–11054
- [31] Guo SP, Guo GC, Wang MS, Zhou JP, Xu G, Wang GJ, Long XF, Huang JS (2009) A series of new infrared NLO semiconductors, ZnY₆Si₂S₁₄, Al_xDy₃ (Si_yAl_{1-y}) S₇, and Al_{0.33}Sm₃Si₇. *Inorg Chem* 48:7059–7065
- [32] Sheng ZH, Shao L, Chen JJ, Bao WJ, Wang FB, Xia XH (2011) Catalyst-free synthesis of nitrogen-doped graphene via thermal annealing graphite oxide with melamine and its excellent electrocatalysis. *ACS Nano* 5:4350–4358
- [33] Xu C, Zeng Y, Rui XH, Xiao N, Zhu JX, Zhang WY, Chen J, Liu WL, Tan HT, Hng HH, Yan QY (2012) Controlled soft-template synthesis of ultrathin C@FeS nanosheets with high-Li-storage performance. *ACS Nano* 6:4713–4721
- [34] Pang SP, Tsao HN, Feng XL, Müllen K (2009) Patterned graphene electrodes from solution-processed graphite oxide

- films for organic field-effect transistors. *Adv Mater* 21:3488–3491
- [35] Yang B, Malkhandi S, Manohar AK, Prakash GKS, Narayanan SR (2014) Organo-sulfur molecules enable iron-based battery electrodes to meet the challenges of large-scale electrical energy storage. *Energy Environ Sci* 7:2753–2763
- [36] Choi SH, Kang YC (2015) Aerosol-assisted rapid synthesis of SnS–C composite microspheres as anode material for Na-ion batteries. *Nano Res* 8:1595–1603
- [37] Zhou F, Xin S, Liang HW, Song LT, Yu SH (2014) Carbon nanofibers decorated with molybdenum disulfide nanosheets: synergistic lithium storage and enhanced electrochemical performance. *Angew Chem Int Ed* 53:11552–11556
- [38] Ha DH, Ly T, Caron JM, Zhang HT, Fritz KE, Robinson RD (2015) A general method for high-performance Li-ion battery electrodes from colloidal nanoparticles without the introduction of binders or conductive-carbon additives: the cases of MnS, Cu_{2-x}S , and Ge. *ACS Appl Mater* 7:25053–25060
- [39] Zhao L, Yu XQ, Yu JZ, Zhou YG, Ehrlich SN, Hu YS, Su D, Li H, Yang XQ, Chen LQ (2014) Remarkably improved electrode performance of bulk MnS by forming a solid solution with FeS—understanding the Li storage mechanism. *Adv Funct Mater* 24:5557–5566
- [40] Guan ES, Li F, Li J, Chang ZR, Li QM, Yuan XZ, Wang HJ (2015) FeS/C composite as high-performance anode material for alkaline nickel-iron rechargeable batteries. *J Power Sources* 291:29–39
- [41] Wei X, Li WH, Shi JA, Gu L, Yu Y (2015) FeS@C on carbon cloth as flexible electrode for both lithium and sodium storage. *ACS Appl Mater* 7:27804–27809
- [42] Liao F, S'wiatowska J, Maurice V, Seyeux A, Klein LH, Zanna S, Marcus P (2015) The influence of the electrolyte on chemical and morphological modifications of an iron sulfide thin film negative electrode. *Phys Chem Chem Phys* 17:619–629
- [43] Xu YX, Li WY, Zhang F, Zhang XL, Zhang WJ, Lee CS, Tang YB (2016) In situ incorporation of FeS nanoparticles/carbon nanosheets composite with an interconnected porous structure as a high-performance anode for lithium ion batteries. *J Mater Chem A* 4:3697–3703
- [44] Ma Y, Asfaw HD, Edström K (2015) A general method to fabricate free-standing electrodes: sulfonate directed synthesis and their Li^+ storage properties. *Chem Mater* 27:3957–3965